



Contents lists available at ScienceDirect

Arabian Journal of Chemistry

journal homepage: www.ksu.edu.sa

Effect of collapse column structure on oxidation and physicochemical characteristics of bituminous coal

Dongjie Hu^{a,b,*}, Zongxiang Li^{a,b}, Yu Liu^{a,b}, Cong Ding^{a,b}, Chuntong Miao^c, Ruting Wei^d^a College of Safety Science and Engineering, Liaoning Technical University, Liaoning 123000, China^b Key Laboratory of Mine Thermodynamic Disasters and Control of Ministry of Education, Liaoning Technical University, Liaoning 123000, China^c China Coal Technology and Engineering Group Shenyang Research Institute, Fushun 113122, China^d Shanxi Shouyang Duan Wang Coal Industry Group Co. Ltd, Shanxi 030600, China

ARTICLE INFO

Keywords:

Collapsed column structure
 Macroscopic physical structure
 Oxidation characteristics
 Microscopic chemical properties
 ReaxFF pyrolysis simulation

ABSTRACT

To investigate the influence of the collapse column structure on the oxidation characteristics of coal, with the aim of preventing mine fires and ensuring the safety of life and property, low-temperature N₂ adsorption, synchronous thermal analysis and enclosed coal oxidation experiments were carried out to analyze the pore structure and macroscopic oxidation characteristics of 3 coal samples (XL1, XL2, XL3) from different affected areas of the collapse column structure in the 1202 working face of Duanwang Mine. ¹³C NMR and XPS experiments were conducted to explore the microscopic differences in chemical structure, surface chemical properties, etc. among them. Meanwhile, coal macromolecular models were constructed for ReaxFF pyrolysis simulation. The results show that compared with the original coal XL2, the pores in coal sample XL3 are more developed. The ignition temperatures for XL1, XL2, and XL3 are 510.74 °C, 492.81 °C, and 482.43 °C, respectively. The initial oxygen consumption rate of coal sample XL3 increased by 150 % compared to XL2, while that of XL1 decreased by 37.5 %. The O/C atomic ratio of XL3 is about 2.0 times that of XL2, and about 2.4 times that of XL1. The A/C ratios (The ratio of aromatic carbon content to alkyl carbon content) of XL1, XL2 and XL3 are 4.866, 3.367 and 3.522, respectively. The molecular formulas for XL1, XL2, and XL3 are C₁₅₄H₈₀O₁₇N₂S₂, C₁₅₆H₉₇O₃₀N₂S₁, and C₁₅₆H₈₇O₃₃N₂S₁, respectively. In the ReaxFF pyrolysis simulation, the occurrence order of indicator gases CO, C₂H₄, C₂H₂ is XL3, XL2, XL1, respectively.

1. Introduction

Coal spontaneous combustion is a major hidden danger in coal mine safety production. The underground geological conditions in coal mines are complex and changeable, which may have different effects on the spontaneous combustion characteristics of coal (Jiang et al., 2020; Shen et al., 2020; Shi et al., 2023). The collapse column is a common structure that destroys the local coal body during the metamorphic process of the coal seam. It has different effects on the mechanical properties and seepage properties of the coal seam in vertical and horizontal directions, thus causing differences in the spontaneous combustion characteristics of the coal body (Yang et al., 2023; Yin et al., 2005; Fang et al., 2022). Therefore, it is of great significance to grasp the influence of collapse column structure on spontaneous combustion characteristics of coal seam for ensuring safe and efficient production of coal mine and

personal safety of miners.

Domestic and foreign scholars have made fruitful achievements in the study of the influence of different geological structural conditions on coal structural characteristics and spontaneous combustion characteristics. Wang et al. (2023) found through research that structural destruction increased the macropore and large pore volume of coal and enhanced the specific surface area, while the micropore volume changed little. Zhang et al. (2020) found that the anticline structure was the main factor affecting the reflectance, adsorption capacity and diffusivity of the coal seam. The adsorption pores and seepage pores in the anticline area were more developed. Zhao et al. (2012) found that geological structures and stresses can enhance the oxidative activity of coal and accelerate spontaneous combustion reactions. There are differences in the spontaneous combustion processes of coal in different structural areas. Through infrared, thermogravimetric, nitrogen adsorption and

* Corresponding author at: College of Safety Science and Engineering, Liaoning Technical University, Liaoning 123000, China.

E-mail addresses: djhu0418@gmail.com (D. Hu), lizx6211@163.com (Z. Li), 784995060@qq.com (Y. Liu), 929087970@qq.com (C. Ding), 1589631416@qq.com (C. Miao), 13546741936@163.com (R. Wei).

<https://doi.org/10.1016/j.arabjc.2024.105649>

Received 24 November 2023; Accepted 22 January 2024

Available online 24 January 2024

1878-5352/© 2024 The Authors. Published by Elsevier B.V. on behalf of King Saud University. This is an open access article under the CC BY-NC-ND license (<http://creativecommons.org/licenses/by-nc-nd/4.0/>).

other experiments, Li et al. (2023) found that the active groups, pore parameters and oxidation activity of coal under the influence of geological structures were greater than those of primary coal. Existing studies have systematically explored the structural characteristics and spontaneous combustion characteristics of coal bodies under different geological structural conditions. This lays a foundation for us to deeply understand the effects of stress and geological structures on coal spontaneous combustion.

This paper takes the 1202 working face of Duanwang Mine as the research object to explore the influence of collapse column structure on coal spontaneous combustion characteristics. According to the field investigation, the overall integrity of the primary coal body in this working face is destroyed by the collapse column structure, which can be roughly divided into the following three types: the pressure-bearing coal XL1 under the collapse column, the undeformed coal XL2 farthest away from the collapse column (unaffected by the collapse column geological structure), and the fragmented coal XL3 inside the fragmented zone and fissure zone around the collapse column (affected). Low-temperature N₂ adsorption experiments (Cheng and Lei, 2021; Wang et al., 2020), synchronous thermal analysis experiments (Yu et al., 2009; Deng et al., 2014), enclosed coal oxygen consumption experiments (Hu and Li, 2022); ¹³C NMR and XPS (Lin et al., 2021; Liu et al., 2019) and other experiments were carried out to explore the differences in macroscopic pore structure, characteristic temperature differences in low-temperature oxidation, room-temperature oxygen consumption characteristics, microscopic chemical structure, surface chemical properties and functional group distribution, etc. among the three coal samples from multiple perspectives. The reasons for the differences in spontaneous combustion tendency of the three coal samples are analyzed. The influence of collapse column on coal spontaneous combustion is concluded to assess the risks of spontaneous combustion in coal affected by different collapse column structures. Corresponding prevention measures can be taken accordingly.

2. Experiments and methods

2.1. Proximate analysis and ultimate analysis of the coal samples

Coal samples were collected from the 15# coal seam at the 1202 working face of Duanwang Mine in Shanxi Province, China. Among them, coal sample XL1 was collected from the relatively intact coal seam under the collapse column filling rocks. XL2 is the original coal sample farthest away from the collapse column (unaffected by the collapse column geological structure). XL3 is inside the fragmented zone and fissure zone around the collapse column (affected).

After the field-collected coal samples were sealed, transported to the laboratory, crushed, and screened to obtain coal samples smaller than 200 mesh, they were vacuum sealed for subsequent experiments. According to the standards GB/T212-2008 and GB/T 31391-2015, proximate analysis and ultimate analysis were performed on the three coal samples using 5E-MAG6600B industrial analyzer produced by Jiaozuo Huacoal Mining Equipment Co., Ltd. in China and Vario EL elemental analyzer produced by Elementar Group in Germany, respectively. The results of proximate analysis and ultimate analysis are shown in Table 1.

It is generally believed that the higher the fixed carbon content in coal, the more combustible components and the higher the calorific value. However, excessive fixed carbon content will also increase the

thermal conductivity of the coal sample, making heat more likely to dissipate to the surroundings, reducing the spontaneous combustion tendency (Genetti et al., 1999). Oxygen content analysis shows that the higher the degree of coal metamorphism, the lower the oxygen content, and the less prone to spontaneous combustion (Wang et al., 2021). Sample XL3 has a high oxygen content and is most prone to spontaneous combustion.

2.2. Low temperature liquid nitrogen adsorption measurements

The pore structure parameters of the coal samples were determined using an ASAP 2460 specific surface area and pore size distribution analyzer produced by Micromeritics Corporation, USA. The low temperature nitrogen adsorption experiment of coal was carried out at 77 K. The test sample is about 5 g of pulverized coal with a particle size less than 0.0750 mm. First, the coal samples were dried and degassed to remove impurities. Then, adsorption analysis was performed on the analyzer using liquid nitrogen adsorption to obtain pore structure related data. The specific surface area of the sample was calculated using the BET theory model, and the pore volume was calculated using the BJH model.

2.3. Synchronous thermal analysis of coal samples

Simultaneous thermal analysis was performed using a STA 449F5-QMS 403D simultaneous thermal analyzer produced by NETZSCH, Germany. The mass of the coal sample used in the experiment was 10 mg. The temperature range was 30–800 °C with a heating rate of 10 °C·min⁻¹. The gas flow rate was 50 mL·min⁻¹ (gas ratio N₂:O₂ = 4:1).

2.4. Oxidation experiment of coal sample in enclosed environment

The enclosed coal oxidation experimental device was independently developed and designed by Professor Li Zongxiang from Liaoning Technical University (Hu and Li, 2022; Li et al., 2017). The pipeline connection diagram and physical map of the device are shown in Fig. 1. The experimental procedure is as follows:

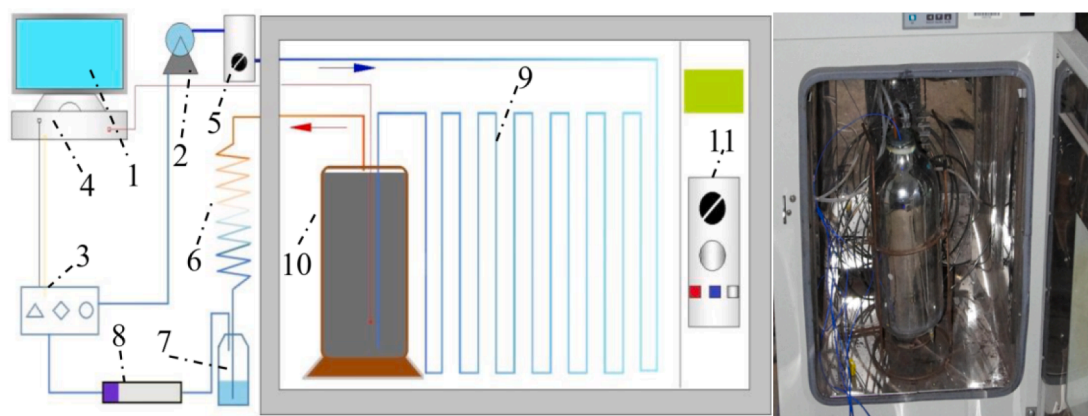
The field-collected coal samples were crushed, screened for coal with a particle size of 0.4–2.4 mm at a specific ratio of 2.0 kg, and charged into the coal sample tank. The pipeline was disconnected for gas washing 10 min before the test to eliminate interference. After the gas washing was completed, the test pipeline was connected to check that the test device was airtight. At the same time, the constant temperature box was run to keep its temperature consistent with the average temperature of the 1202 working face. The data acquisition software was opened to record the O₂ and CO concentration data. The experiment was stopped when the changes in the data curves tended to be stable.

2.5. X-ray photoelectron spectroscopy test

The X-ray photoelectron spectra of coal samples were tested using an ESCALAB Xi + X-ray photoelectron spectrometer produced by Thermo Fisher Scientific, USA. The vacuum degree was 8×10^{-10} Pa. The excitation source was Al K α radiation. Signal accumulation was performed in 10 cycles, with a step size of 0.05 eV and dwell time of 40–50 ms.

Table 1
Proximate and ultimate analysis.

Coal sample	Proximate analysis (%)				Ultimate analysis (%)				
	Moisture	Ash	Volatile	Fixed carbon	C	H	O	N	S
XL1	0.99	8.31	9.16	81.54	81.97	3.49	10.94	1.22	2.38
XL2	0.89	15.27	15.02	68.82	74.43	3.85	19.01	1.45	1.26
XL3	0.82	13.95	18.16	67.07	73.24	3.41	21.24	1.08	1.03



1 is a computer, 2 is an air pump, 3 is a gas concentration sensor, 4 is a data collector, 5 is a flow meter, 6 is a condensing tube, 7 is a water collecting bottle, 8 is a drying tube, 9 is a preheating pipeline, 10 is a coal sample tank, and 11 is a constant temperature box.

Fig. 1. Schematic diagram of experimental device for oxygen consumption during coal sample oxidation in enclosed environment.

2.6. Nuclear magnetic resonance carbon spectrum test

The carbon spectrum analysis was conducted in accordance with the SY/T 5777-1995 standard using a high-precision Bruker 400 MHz nuclear magnetic resonance spectrometer, manufactured in Switzerland. Utilizing a high-resolution double-resonance MAS probe with a diameter

of 4.0 mm, the rotor operated at a speed of 10 kHz, pulse width of 4 μ s, pulse delay time of 1 s, and contact time of 2 ms. A total of 10,000 scans were conducted to obtain carbon atomic information from the coal sample.

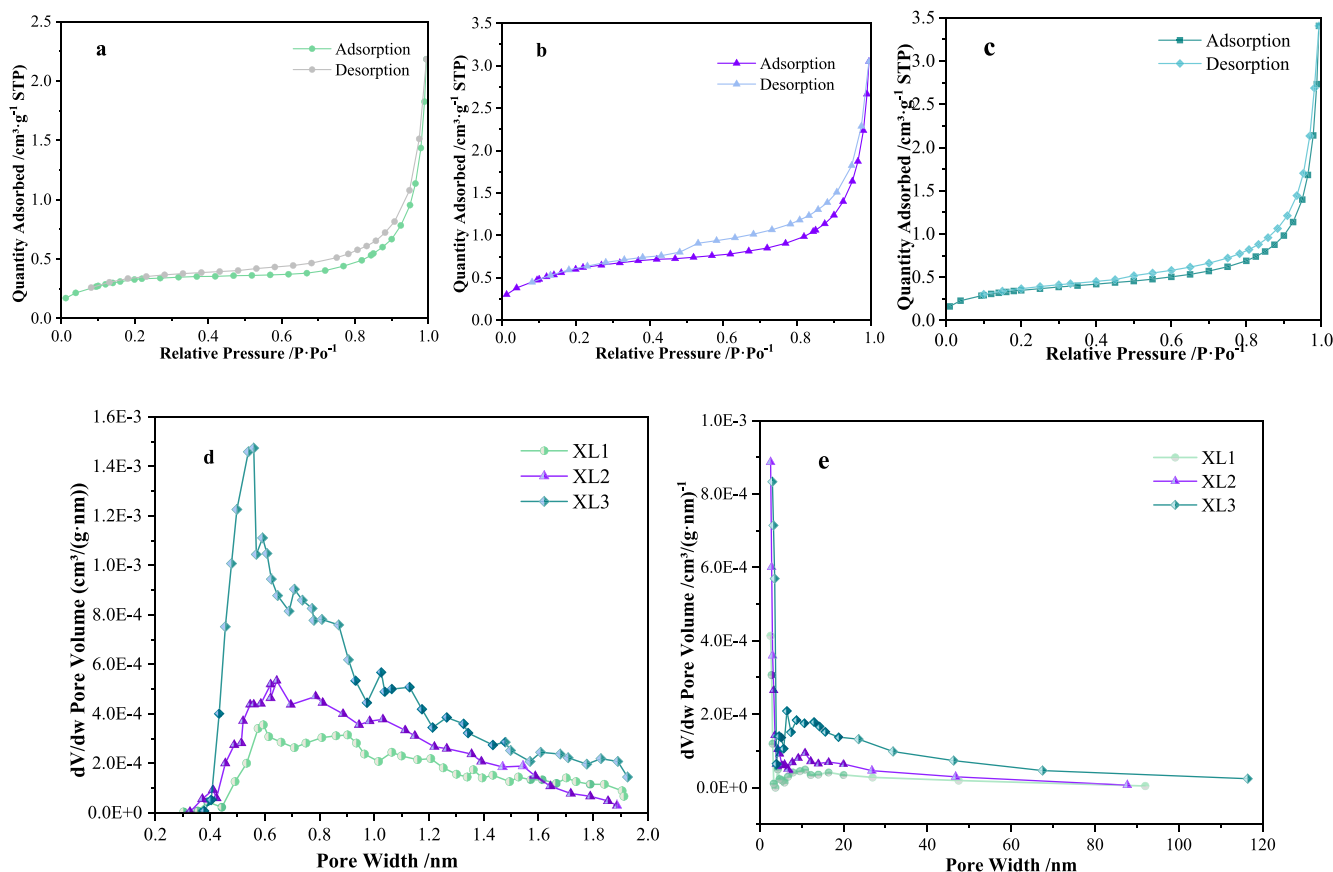


Fig. 2. Results of low temperature N_2 adsorption test of coal samples (a is the Isothermal adsorption-desorption curve of XL1, b is the Isothermal adsorption-desorption curve of XL2, c is the Isothermal adsorption-desorption curve of XL3, d and e is the distribution curve of pore volume of coal).

2.7. Coal molecular ReaxFF pyrolysis simulation

The coal molecular structure was constructed using MestReNova software. The 3 coal molecular structures were optimized using Material Studio to construct a reactive system with a density of $0.5 \text{ g}\cdot\text{m}^{-3}$ containing coal and oxygen molecules. The lowest energy configuration was obtained after optimization. In the ReaxFF force field of the LAMMPS molecular simulation software, the constructed mixed system model was calculated by molecular reaction dynamics under the conditions of NVE ensemble, Berendsen temperature control, time step of 0.2 fs, heating rate of $5 \text{ K}\cdot\text{ps}^{-1}$, temperature range of 300–5000 K. The types and quantities of reaction products at every 2500 time steps were recorded.

3. Results and discussion

3.1. Pore size distribution characteristics

Micropores can adsorb and store more gases. When the oxygen concentration in the micropores increases, it can easily promote the oxidation reaction of coal and thus increase the risk of coal spontaneous combustion. In addition, micropores can also provide a larger specific surface area and provide more adsorption and catalytic active sites, which are the main sites for the initial reaction of coal low temperature oxidation (Schure et al., 1985). Mesopores can provide some oxygen diffusion channels. Under normal circumstances, medium pores are unlikely to directly initiate spontaneous combustion, but they can affect the permeability of coal. When the quantity is small, they may hinder the flow of oxygen and make coal spontaneous combustion more difficult to occur (Okolo et al., 2015).

Fig. 2 shows the results of low temperature N_2 adsorption tests of the three coal samples. Combined with the pore structure parameters of coal samples obtained from low temperature N_2 adsorption as shown in Table 2, it can be analyzed that compared with coal sample XL2, i.e. the original coal unaffected by the collapse column structure, the specific surface area, average pore diameter, micropore volume and BJH pore volume of coal sample XL1 under the collapse column rock decreased by 21.2 %, 38.9 %, 29.3 % and 18.1 % respectively, while those of the fragmented coal XL3 around the collapse column increased by 116.9 %, 25.6 %, 69.7 % and 39.5 % respectively. These data indicate that XL3 has a larger surface area, larger pore volume, larger average pore diameter and more micropore structures than the original coal XL2, and has stronger spontaneous combustion tendency compared to XL2. In contrast, the pore structure of XL1 is relatively small with a smaller surface area, and its spontaneous combustion tendency may be weaker.

3.2. Simultaneous thermal analysis results

According to (Yu et al., 2009; Ding et al., 2022), the TG-DTG & DSC curves of the three coal samples obtained from the simultaneous thermal analysis experiments are shown in Fig. 3. The DTG curve reflects the mass loss rate of the coal sample. The lower the peak, the stronger the combustion reactivity. It can be seen from the figure that the peak values of the DTG curves of the three coal samples XL1, XL2 and XL3 are about $-31 \text{ mW}\cdot\text{mg}^{-1}$, $-40 \text{ mW}\cdot\text{mg}^{-1}$, $-46 \text{ mW}\cdot\text{mg}^{-1}$, respectively. Therefore, in terms of combustion reaction activity, the flammability sequence of

Table 2

Pore structure parameters of coal samples obtained from low temperature N_2 adsorption.

Coal sample	BET Surface Area/ $\text{m}^2\cdot\text{g}^{-1}$	Adsorption average pore diameter/nm	HK microporous pore volume/ $10^{-3}\cdot\text{cm}^3\cdot\text{g}^{-1}$	BJH desorption cumulative volume of pores/ $10^{-3}\cdot\text{cm}^3\cdot\text{g}^{-1}$
XL1	0.829	8.266	3.783	2.715
XL2	1.053	13.533	5.355	3.320
XL3	2.281	16.995	9.086	4.629

the coal samples is XL3 the strongest, XL2 the second, and XL1 the weakest. The DSC curve represents the heat released by the coal sample during the experiment. The larger the peak value, the stronger the heat release reaction. The lowest peak of the DSC curve of coal sample XL3 indicates that its heat release reaction is the most intense.

Table 3 shows relevant data on the characteristic combustion temperatures of coal samples. T_0 is the starting temperature of the experiment, T_1 is the point temperature at which the water loss ends, T_2 is the temperature at the highest point of oxygen gain, T_3 is the temperature at the ignition point, T_4 is the temperature at the maximum weight loss rate, and T_5 is the burnout temperature. The ignition temperatures T_3 of XL1, XL2 and XL3 are $510.74 \text{ }^\circ\text{C}$, $492.81 \text{ }^\circ\text{C}$ and $482.43 \text{ }^\circ\text{C}$, respectively. The temperatures T_4 at the maximum weight loss rate are $554.69 \text{ }^\circ\text{C}$, $542.33 \text{ }^\circ\text{C}$ and $533.92 \text{ }^\circ\text{C}$, respectively. The above data analysis shows that compared with XL2, coal sample XL3 is more prone to spontaneous combustion, because its thermal decomposition or combustion reactions occur at lower temperatures and at faster rates, releasing more heat (Yu et al., 2009; Ding et al., 2022).

3.3. Results of enclosed coal sample oxygen consumption test

The algorithmic principle used to determine experimental parameters is elaborated as follows (Hu and Li, 2022). It is hypothesized that the volume fraction of oxygen concentration $C(\tau)$ in the sealed vessel adheres to the distribution of a negative exponential function:

$$c(\tau) = c_b + (c_0 - c_b) \cdot e^{-\lambda_c \tau} \quad (1)$$

where C_0 is the initial volume fraction of oxygen, %; λ_c is the decay rate of the oxygen volume fraction, s^{-1} ; C_b is the stable oxygen volume fraction value, %; τ is the oxidation time, s.

By differentiating Eq. (1) with respect to time τ :

$$\gamma = \begin{cases} 0, & (c(\tau) < c_b) \\ -0.4464\lambda_c(c_0 - c_b)e^{-\lambda_c \tau}, & (c(\tau) \geq c_b) \end{cases} \quad (2)$$

where 0.4464 is the amount of substance per unit volume, $\text{mol}\cdot\text{m}^{-3}$; γ is the volumetric oxygen consumption rate, $\text{mol}\cdot(\text{m}^3\cdot\text{s})^{-1}$.

Substituting Eq. (1) into Eq. (2) yields can be obtained:

$$\gamma = 0.4464\lambda_c[c(\tau) - c_b] \quad (3)$$

It can be seen from Fig. 4, the results of the enclosed oxygen consumption test of two coal samples, that the change curve of oxygen volume fraction with time obtained from the enclosed oxygen consumption test shows an exponential decay distribution. The volumetric oxygen consumption rate of the coal sample is positively correlated with the oxygen volume fraction. As the reaction between coal samples XL1, XL2, XL3 and oxygen in the enclosed tank, the oxygen volume fractions of coal samples XL1, XL2, XL3 gradually stabilized at 10 %, 6 %, 3 % respectively. Affected by the collapse column structure, the initial oxygen consumption rate (at the beginning of the experiment) of coal sample XL3 increased by 150 % compared to the original coal XL2, while the initial oxygen consumption rate of XL1 decreased by 37.5 % compared to the original coal XL2.

3.4. XPS test results of coal samples

XPS testing can detect the surface elemental composition and chemical states of samples. For coal samples, it can mainly reflect the types and contents of oxygen-containing functional groups on the sample surface (Prins et al., 2007). Generally speaking, the more oxygen-containing functional groups on the coal sample surface, especially samples with high oxygen content and abundant acidic oxygen-containing functional groups, the stronger its spontaneous combustion tendency. As shown in Fig. 5, the O/C atomic ratios of coal samples XL1, XL2 and XL3 are approximately 0.0784, 0.0915 and 0.1871, respectively. The O/C atomic ratio reflects the overall oxidation degree of the

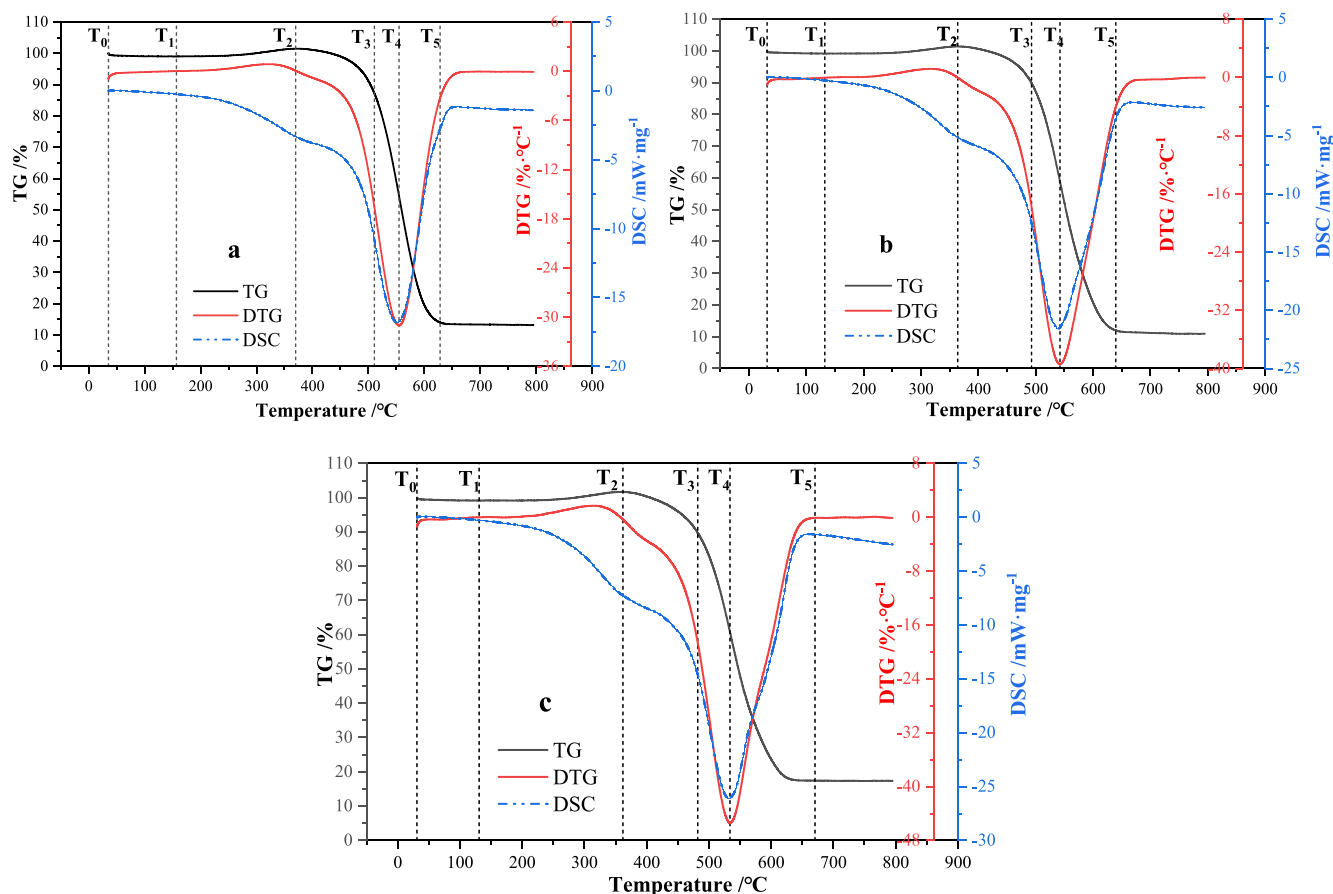


Fig. 3. TG-DTG & DSC curves of coal samples (a is XL1, b is XL2, c is XL3).

Table 3

Characteristic combustion temperatures of coal samples (°C).

Coal sample	T ₀	T ₁	T ₂	T ₃	T ₄	T ₅
XL1	32.00	156.82	370.05	510.74	554.69	628.18
XL2	32.00	132.27	363.95	492.81	542.33	639.74
XL3	32.00	130.70	361.92	482.43	533.92	670.43

sample. The larger the O/C ratio, the deeper the oxidation degree of coal, and the more oxygen-containing functional groups, making it easier to combust spontaneously (Atesok et al., 2002).

Table 4 shows the peak fitting information in the C 1s, O 1s, N 1s, and S 2p binding energy regions for the three coal samples. The number of oxygen-containing functional groups is often related to the spontaneous combustibility of coal. Since the weights of the three coal samples used in the XPS test were the same, the absolute content of oxygen-containing functional groups in the coal sample XPS results can be compared to

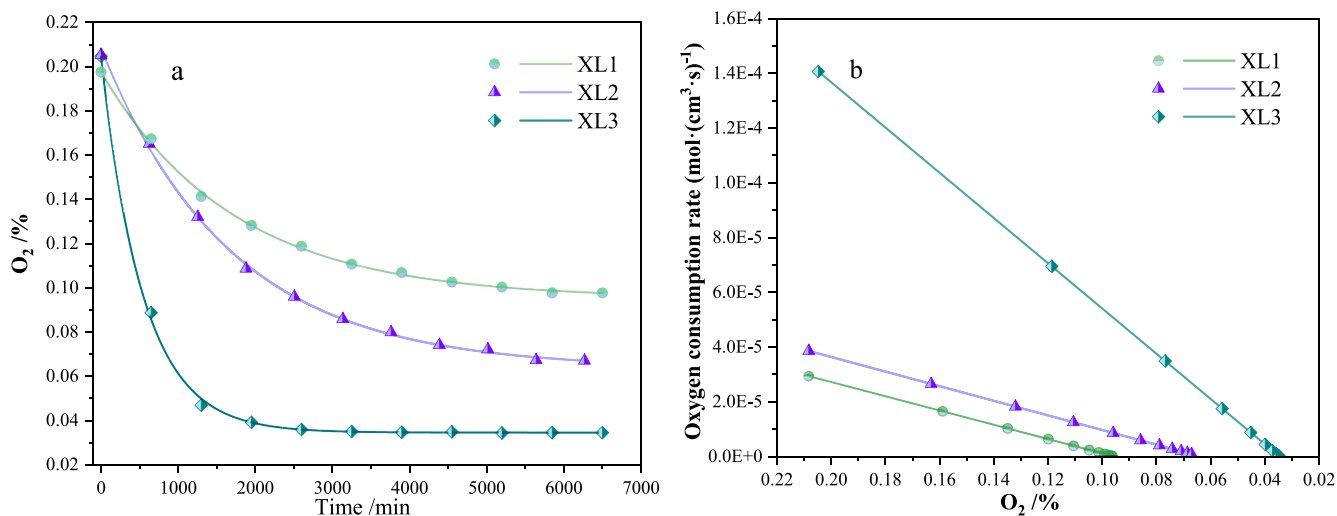


Fig. 4. Results of closed spontaneous combustion tests of coal samples (a is the oxygen volume fraction change curve of coal samples, and b is the oxygen consumption rate of coal samples).

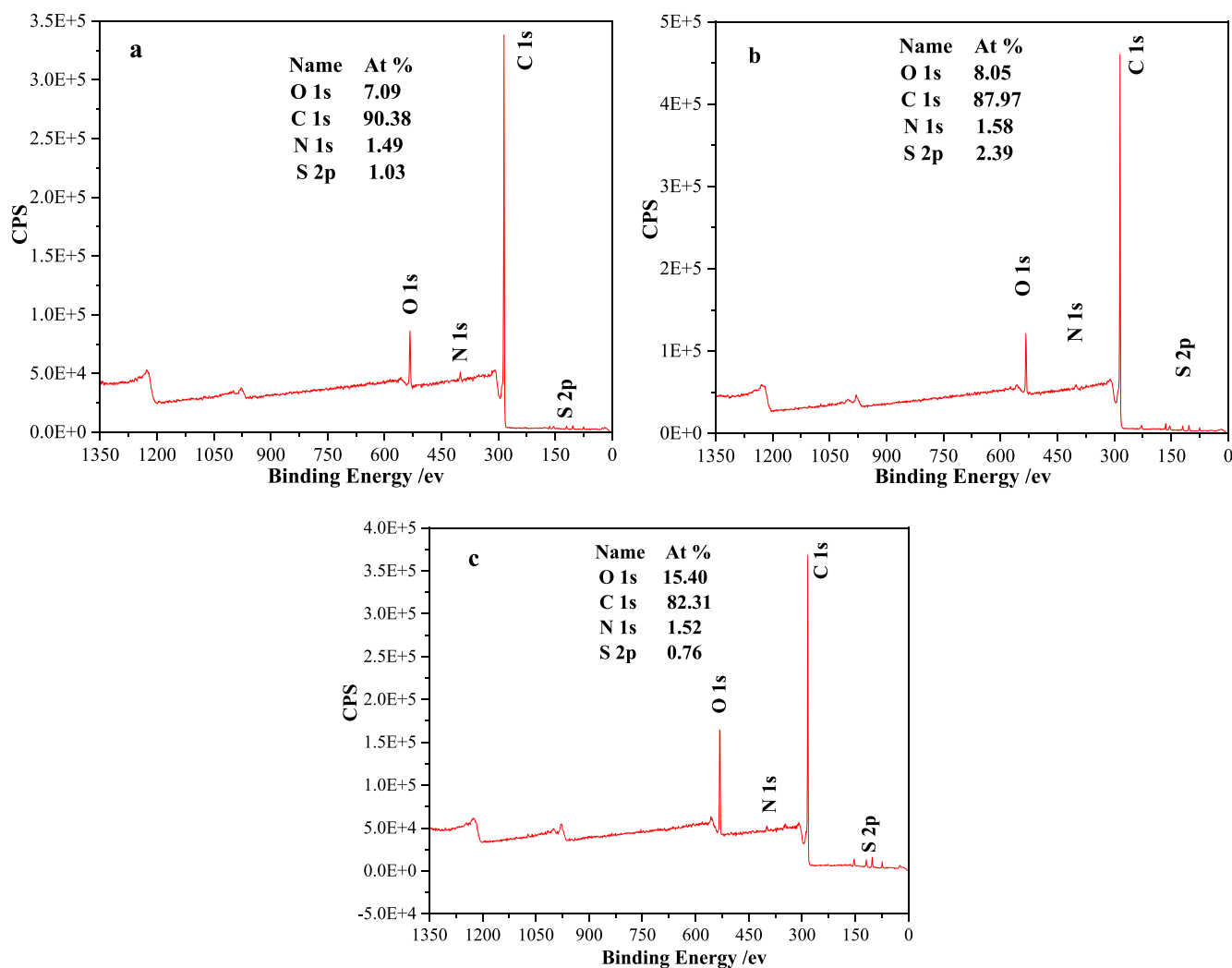


Fig. 5. XPS test results of coal samples (a is XL1, b is XL2, c is XL3).

determine the spontaneous combustibility of coal. By summing the area values of the oxygen-containing functional group peaks corresponding to C 1s and O 1s (the main types of oxygen-containing functional groups are C–O, C=O, COO⁻), the absolute contents of oxygen-containing functional groups in coal samples XL1, XL2 and XL3 from small to large were 172173.69, 182161.17 and 191109.22, respectively. In addition, carbonyl and carboxylate functional groups account for the largest proportion of oxygen-containing functional groups in coal sample XL3, indicating that coal sample XL3 has the strongest spontaneous combustion tendency.

3.5. ¹³C NMR test results of coal samples

In analyzing the strength and weakness of coal spontaneous combustibility, the content of aromatic carbon and alkyl carbon may affect the spontaneous combustibility of coal. Aromatic compounds are usually cyclic structures composed of carbon and hydrogen atoms, with the carbon atoms in these rings arranged in alternating single and double bonds, forming a conjugated π electron system that gives aromatic compounds relatively high stability and resistance to chemical reactions (Yuan et al., 2016). Alkyl carbons are usually more likely to undergo oxidation reactions with oxygen because they contain saturated carbon–carbon single bonds and have higher chemical reactivity. Therefore, coal containing more alkyl carbons often has a higher tendency for spontaneous combustion to some extent (Shi et al., 2018; Hu

et al., 2024). The chemical shifts between 0 and 50 ppm are usually associated with saturated aliphatic hydrocarbons (alkyl carbons), and aromatic carbon peaks are usually between 90 and 165 ppm.

The ratio of aromatic carbon content to alkyl carbon content is called the A/C ratio. A high A/C ratio indicates a relatively high content of aromatic carbon and a relatively low content of alkyl carbon. In this case, the molecular structure of coal may be more ordered and have a lower tendency for spontaneous combustion. According to the ¹³C NMR test results of coal samples in Fig. 6 and Table 5, the A/C ratios of coal samples XL1, XL2 and XL3 are 4.866, 3.367 and 3.522, respectively, and the area percentages of oxygen-containing functional group corresponding peaks are 30.54 %, 27.74 % and 30.42 %, respectively. It can be concluded that XL1 is the most difficult to combust spontaneously. The A/C ratio of coal sample XL2 is slightly higher than that of coal sample XL3, but the oxygen-containing functional group content is lower than that of coal sample XL3. Therefore, through comprehensive comparative analysis, it is concluded that the spontaneous combustibility of coal sample XL3 is stronger than XL2.

3.6. Coal molecular construction and pyrolysis process simulation

3.6.1. Construction of coal molecular models

According to the elemental analysis results in Table 1, the atomic ratios of the three coal samples were calculated, as shown in Table 6. With reference to the methods of scholars in constructing coal molecular

Table 4
Coal sample XPS test binding energy attribution statistics.

Number	XL1				XL2				XL3				Attribution	
	Peak position /eV	FWHM /eV	Area	Relative area /%	Peak position /eV	FWHM /eV	Area	Relative area /%	Peak position /eV	FWHM /eV	Area	Relative area /%		
a/C 1	1	284.80	1.21	190990.00	60.21	284.80	1.21	141860.00	55.25	284.80	1.20	174860.00	67.50	C-C/C-H
	2	285.38	2.31	57689.61	18.19	285.41	2.11	60572.32	23.59	285.84	0.84	9553.76	3.69	C-O
	3	288.87	7.05	68522.56	21.60	288.68	6.95	54340.04	21.16	286.37	1.69	14936.82	5.77	C = O
b/N 1	1	395.20	0.77	536.00	5.88	397.12	1.52	559.94	5.99	288.71	7.44	59698.64	23.05	COO-
	2	398.73	1.15	2369.60	26.07	398.51	0.54	2512.47	26.90	397.54	1.40	2057.41	28.50	Metal nitrides
	3	400.43	1.31	2594.11	28.56	400.26	1.75	5980.07	64.08	399.31	1.20	2907.08	40.31	Pyrrrole
	4	402.12	2.56	2893.17	31.89					400.58	5.36	2149.88	29.83	Pyrrrole Oxidised
c/O 1	5	406.63	1.43	687.98	7.60	406.44	0.51	281.61	3.03	408.52	0.49	96.87	1.35	nitrogen
	1	532.90	2.43	41415.76	90.11	532.70	2.28	60307.51	89.68	532.74	2.26	106920.00	100.00	Nitrate
	2	534.14	6.11	4545.76	9.89	533.89	4.95	6941.30	10.32					C-O
d/S 2p	1	164.08	0.91	3632.43	59.49	164.05	1.08	1197.48	58.42	158.87	0.74	285.68	8.92	C = O
	2	165.07	1.27	1162.67	19.05	165.09	1.45	494.15	24.12	162.95	1.12	1634.78	51.12	Metal sulfide
	3	165.50	0.81	679.34	11.13					164.26	0.81	282.41	8.84	Thiophene
	4	167.92	1.79	629.74	10.33	168.63	2.17	357.02	17.46					
	5									167.91	2.67	993.38	31.13	Metal sulfate

models (Hu et al., 2024; Gao, 2021; Zhang, 2022), combined with the XPS and ^{13}C NMR experimental data, large molecular models of the three coal samples were constructed. The MestReNova was used to calculate the ^{13}C NMR spectra of these large molecular structure models to match the experimental spectra shown in Fig. 6 as much as possible. The constructed 3D molecular models of the three coal samples are shown in Fig. 7.

3.6.2. ReaxFF pyrolysis simulation of coal samples

The macroscopic oxidation characteristics of coal samples XL1, XL2 and XL3 were explored through simultaneous thermal analysis and closed coal oxidation experiments. To more comprehensively analyze the strength and weakness of spontaneous combustion ability of the three coal samples, the ReaxFF reactive force field was utilized to simulate the chemical reactions, structural evolution of coal, and product generation during high temperature reactions and combustion processes of coal samples at the atomic scale. Fig. 8 shows the coal-oxygen reaction systems of the three coal samples and the changes in coal molecular structure during pyrolysis (Hu et al., 2024; Ding et al., 2023).

Combining the analysis of Fig. 8, the pyrolysis of coal is a stepwise and complex process, involving various reactions such as removal of functional groups, hydrocarbon cracking and aromatic ring recombination. It can be roughly divided into three stages:

The first stage is the low temperature cracking stage (temperature is generally below 200 °C):

Non-covalent weak bonds between coal molecules break (such as van der Waals forces), removing adsorbed water and some functional groups. Aromatic rings condense to form polycyclic aromatic hydrocarbon structures. Hydrocarbon crosslinking occurs and hydrocarbon chains interconnect to form network structures. The original functional groups undergo polymerization reactions to generate products such as ethers and aldehydes.

The third stage is the recombination stage (temperature exceeds 500 °C):

Aromatic rings polymerize and recombine to form aromatic clusters. Free radicals interconnect to form graphitized structures. Residual hydrocarbons undergo thermal cracking to generate low-carbon gases like CH_4 . Amorphous carbonaceous substances are formed.

Fig. 9 shows the generation patterns of four gases CO_2 , CO , C_2H_2 and C_2H_4 in the reaction dynamics simulations of the three coal samples.

It can be observed that the generation times of these three gases CO , C_2H_2 and CO_2 for coal sample XL3 are significantly earlier than the other two coal samples (XL1 has the latest generation times), but the contents of these three gases in XL3 are relatively lower than those of raw coal XL2 and compacted coal XL1. The initial generation times and contents of C_2H_4 for the three coal samples are close but XL3 appears earliest. It is inferred that XL3 is the most prone to spontaneous combustion.

4. Conclusions

Collapse column structure changes the stress distribution in coal seams, thereby affecting the spontaneous combustion characteristics of surrounding coal. This study explores the oxidation characteristics and physicochemical features of compacted coal sample below the collapse column structure (XL1), raw coal sample farther away from the collapse column structure (XL2), and coal sample in the fracture zone around the collapse column structure (XL3), from macroscopic and microscopic perspectives. The following conclusions are obtained:

- (1) For coal seams under collapse column structure, a large number of fracture zones and fissures are formed around the caving center, enhancing the local permeability of the coal seam. Vertically, under the influence of caving and formation stresses, the coal below the caving is compressed and deformed with decreased porosity and permeability.

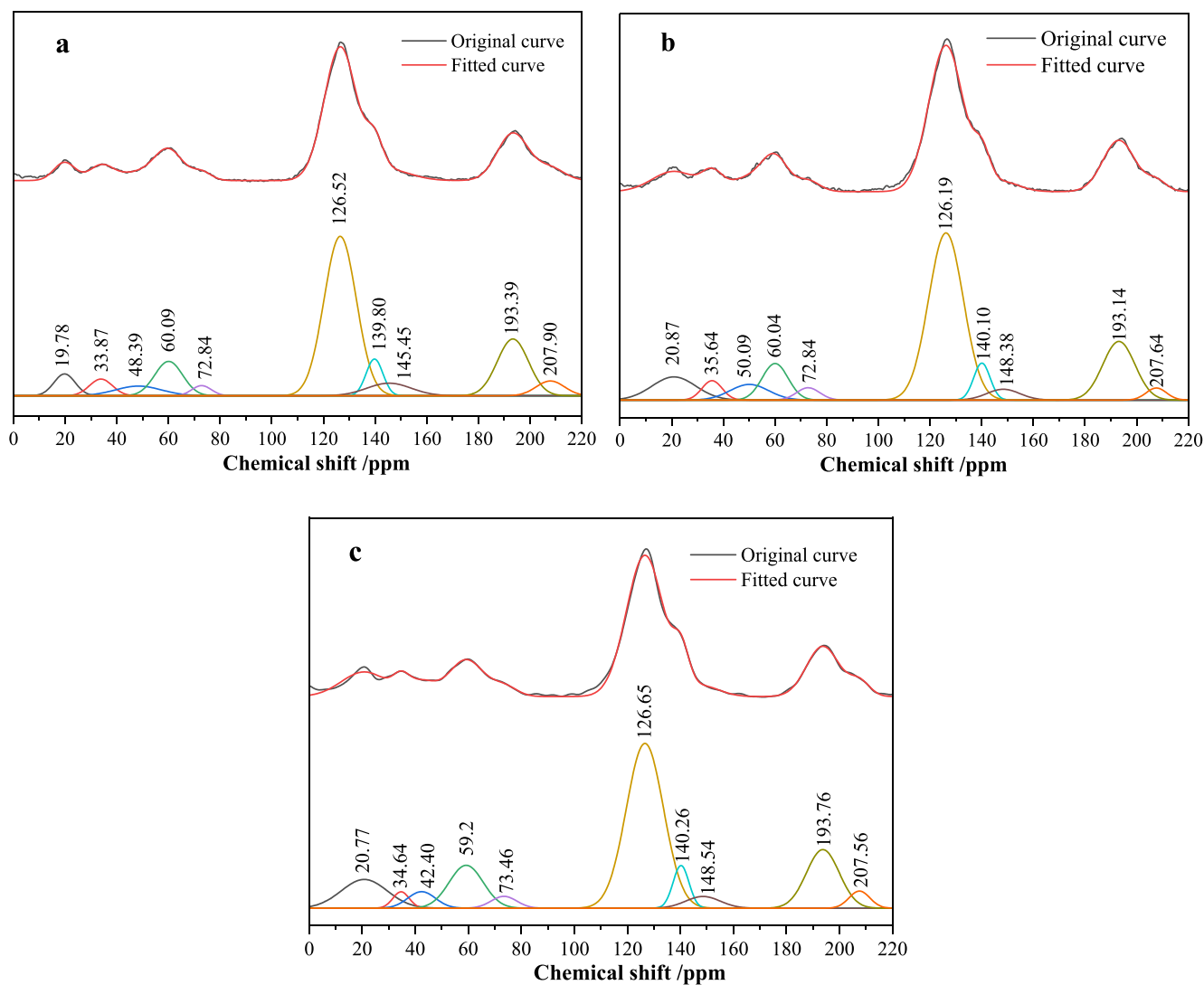


Fig. 6. ^{13}C NMR spectra and peak fitting results (a is XL1, b is XL2, c is XL3).

Table 5

Absorption peak parameters of coal sample ^{13}C NMR.

Peak Number	XL1				XL2				XL3				Attribution
	Center	FWHM	Anlytc Area	Area/%	Center	FWHM	Anlytc Area	Area/%	Center	FWHM	Anlytc Area	% Area	
1	19.78	9.70	5.57×10^8	4.24	20.87	19.93	8.49×10^8	8.36	20.77	20.37	1.80×10^9	9.92	Benzylic carbon
2	33.87	10.48	4.60×10^8	3.51	35.64	9.16	3.27×10^8	3.22	34.64	7.25	3.65×10^8	2.02	Methylene carbon
3	48.39	21.08	5.37×10^8	4.09	50.09	17.55	5.05×10^8	4.97	42.40	12.28	6.23×10^8	3.45	Quaternary and secondary methyl carbon
4	60.09	12.69	1.15×10^9	8.74	60.04	11.78	7.92×10^8	7.80	59.22	15.10	1.99×10^9	10.98	Methoxy and oxygen-substituted methylene carbon
5	72.84	8.90	2.38×10^8	1.81	72.84	10.54	2.39×10^8	2.35	73.46	11.40	4.15×10^8	2.30	Oxygen-substituted aliphatic carbon in rings
6	126.52	14.69	6.15×10^9	46.88	126.19	15.80	4.85×10^9	47.78	126.65	16.49	8.33×10^9	46.03	Protonated aromatic carbon
7	139.80	7.67	7.40×10^8	5.64	140.10	7.48	5.08×10^8	5.00	140.26	7.07	9.25×10^8	5.11	Aliphatic carbon attached to aromatic ring
8	145.45	20.14	6.67×10^8	5.09	148.38	14.97	2.98×10^8	2.94	148.54	15.34	5.53×10^8	3.06	Oxygen-substituted aromatic carbon
9	193.39	14.23	2.12×10^9	16.17	193.14	14.67	1.58×10^9	15.57	193.76	14.56	2.62×10^9	14.46	Carbonyl carbon
10	207.90	12.87	5.01×10^8	3.82	207.64	9.24	2.05×10^8	2.02	207.56	9.22	4.86×10^8	2.68	

Table 6

Atomic ratio of coal sample.

Coal sample	H/C	O/C	N/C	S/C
XL1	0.520128	0.110583	0.012702	0.010975
XL2	0.620717	0.191556	0.016698	0.006348
XL3	0.558711	0.217504	0.012639	0.005274

(2) The ignition point temperatures T_3 of coal samples XL1, XL2 and XL3 are 510.74 °C, 492.81 °C and 482.43 °C, respectively; the temperatures T_4 at maximum weight loss rate are 554.69 °C, 542.33 °C and 533.92 °C, respectively; and the peak values of DTG curves are about $-31 \text{ mW}\cdot\text{mg}^{-1}$, $-40 \text{ mW}\cdot\text{mg}^{-1}$ and -46

$\text{mW}\cdot\text{mg}^{-1}$, respectively. Results of closed spontaneous combustion tests show the oxygen volume fractions of XL1, XL2 and XL3 gradually stabilize at 10 %, 6 % and 3 %, respectively. The initial oxygen consumption rate of XL3 (at the start of the test) increased by 150 % compared to raw coal XL2, while XL1 decreased by 37.5 %. Therefore, from the perspective of low temperature coal oxidation, the combustibility order of the samples is XL3 > XL2 > XL1.

(3) XPS results show the O/C atomic ratios of XL1, XL2 and XL3 are approximately 0.0784, 0.0915 and 0.1871, respectively, and the absolute oxygen-containing functional group contents range from 172173.69 to 191109.22. ^{13}C NMR results show the A/C ratios of XL1, XL2 and XL3 are 4.866, 3.367 and 3.522, respectively.

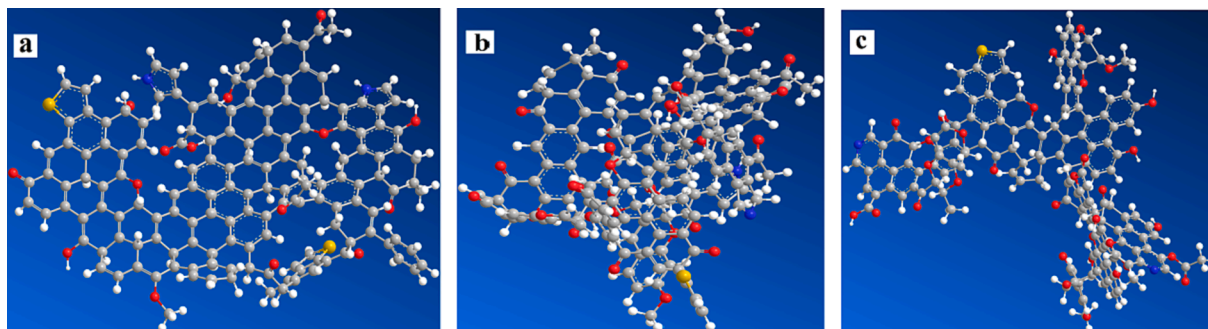


Fig. 7. 3D molecular models of coal samples (a is XL1, b is XL2, c is XL3).

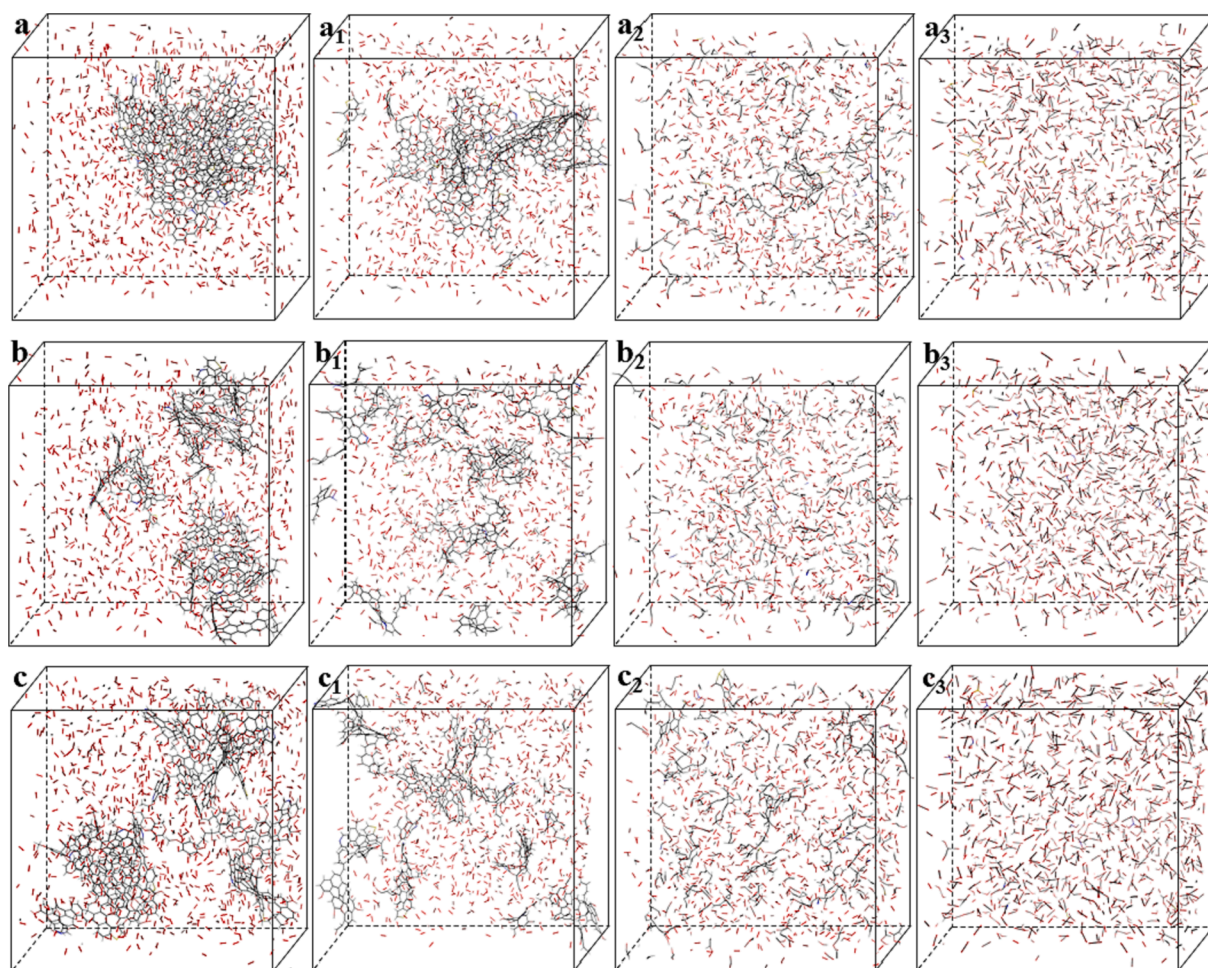


Fig. 8. Coal-oxygen reaction systems and pyrolysis processes (a, b, c are initial models of reaction systems).

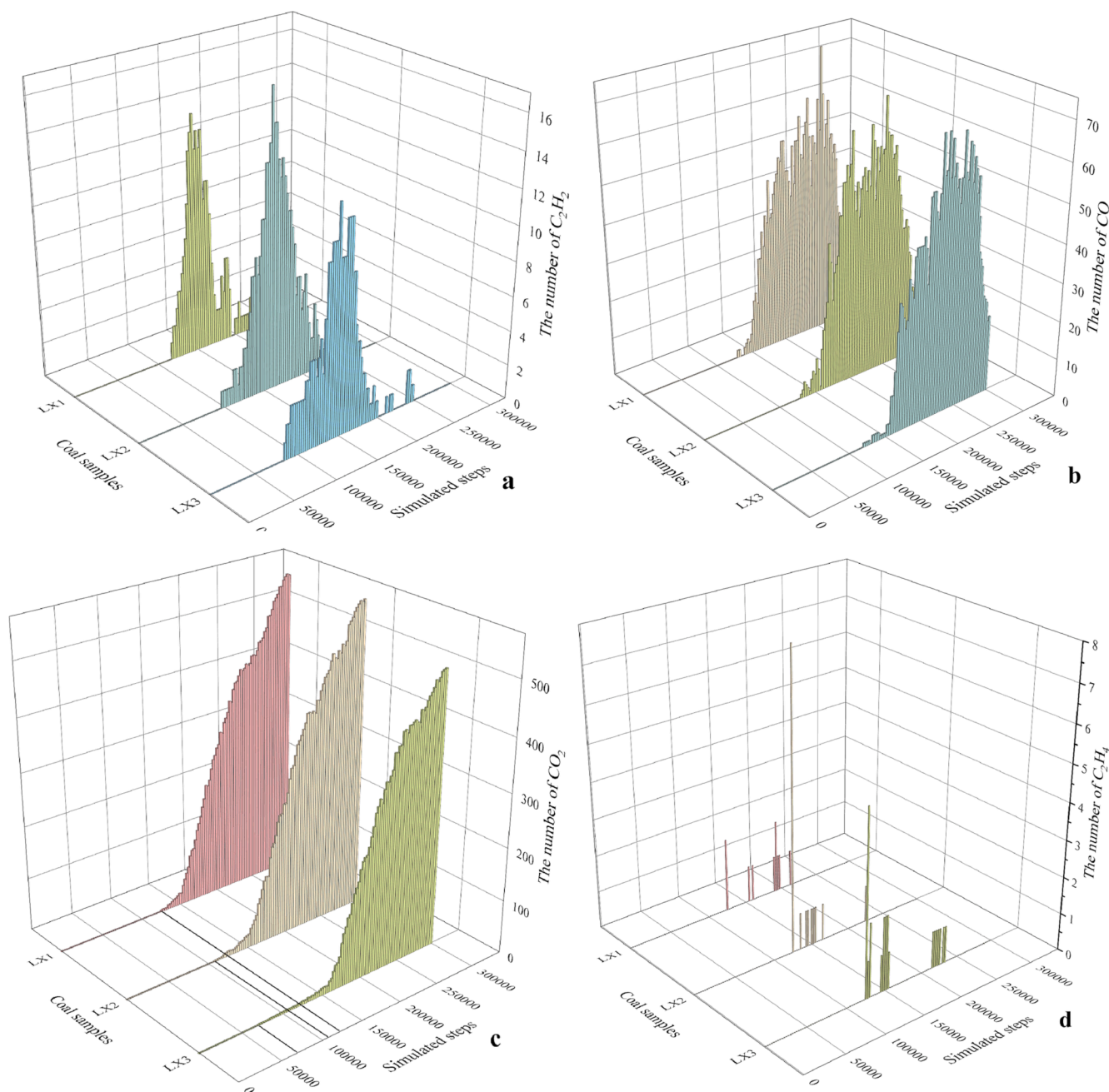


Fig. 9. Generation rule of indicator gas obtained by ReaxFF pyrolysis (a is C_2H_2 , b is CO, c is CO_2 , d is C_2H_4).

ReaxFF pyrolysis simulations of the three coal samples indicate earlier generation times of CO_2 , CO, C_2H_2 and C_2H_4 for LX3 compared to raw coal LX2 and compacted coal LX1.

Declaration of competing interest

The authors declare that they have no known competing financial interests or personal relationships that could have appeared to influence the work reported in this paper.

Acknowledgments

The authors acknowledge the financial support from the National Natural Science Foundation of China (51774170).

References

- Atesok, G., Boylu, F., Sirkeci, A.A., 2002. The effect of coal properties on the viscosity of coal–water slurries[J]. *Fuel* 81 (14), 1855–1858.
- Cheng, Y.P., Lei, Y., 2021. Causality between tectonic coal and coal and gas outbursts[J]. *J. China Coal Soc.* 46 (1), 180–198.
- Deng, J., Zhao, J.Y., Zhang, Y.N., Wu, K., Zhang, D.D., Zhao, M.Y., 2014. Experimental study on spontaneous combustion characteristics of secondary oxidation of Jurassic coal [J]. *China Safety Sci. J.* 24 (01), 34–40.
- Ding, C., Li, Z.X., Wang, J.R., Gao, D.M., 2022. Experimental research on the spontaneous combustion of coal with different metamorphic degrees induced by pyrite and its oxidation products[J]. *Fuel* 318, 123642.
- Ding, C., Li, Z.X., Hu, D.J., Miao, C.T., Lu, B., Gao, D.M., 2023. Construction of macromolecular model and analysis of oxygen absorption characteristics of Hongyang No. 2 coal mine[J]. *Arab. J. Chem.* 16 (5), 104662.
- Fang, J.W., Wang, B., Liu, S.D., Zhang, J., Huang, L.Y., Wang, Y.F., 2022. Full-waveform inversion and its application in imaging of complex collapse columns in coal seam [J]. *J. China Univ. Min. Technol.* 51 (05), 863–872.
- Gao, D., 2021. Research on Gas Chemical Generating Mechanism in the Process of Coal and Gas Outburst [D]. Liaoning Technical University.

- Genetti, D., Fletcher, T.H., Pugmire, R.J., 1999. Development and application of a correlation of ^{13}C NMR chemical structural analyses of coal based on elemental composition and volatile matter content[J]. *Energy Fuel* 13 (1), 60–68.
- Hu, D.J., Li, Z.X., 2022. Dynamic distribution and prevention of spontaneous combustion of coal in gob-side entry retaining goaf[J]. *PLoS One* 17 (5), e0267631.
- Hu, D.J., Li, Z.X., Liu, Y., Li, L., 2024. Construction of macromolecular structure in KunNing coal and analysis of Macro-Micro oxidation characteristics[J]. *Arab. J. Chem.* 17 (1), 105499.
- Hu, D.J., Li, Z.X., Liu, Y., Ding, C., Miao, C.T., Wang, H.W., 2024. Coal pyrolysis law and mechanism of index gas generation in Linsheng Mine[J]. *J. Mol. Struct.* 1297, 136912.
- Jiang, B., Zhao, Y., Lin, B., 2020. Effect of faults on the pore structure of coal and its resultant change on gas emission[J]. *J. Pet. Sci. Eng.* 195, 107919.
- Li, Z.X., Liu, Y., Wu, B.D., Zhang, H.B., Jia, J.Z., Chen, X.K., 2017. Critical oxygen volume fraction of smothering quenched zone based on closed oxygen consumption experiment [J]. *J. China Coal Soc.* 42 (07), 1776–1781.
- Li, Z.X., Zhang, M.Q., Yang, Z.B., Liu, Y., Ding, C., 2023. Effect of fault structure on the structure and oxidative spontaneous combustion characteristics of coal [J]. *J. China Coal Soc.* 48 (03), 1246–1254.
- Lin, H.L., Wang, Y.H., Gao, S.S., Xue, Y., Yan, C.Y., Han, S., 2021. Chemical structural characteristics of high inertinite coal[J]. *Fuel* 286, 119283.
- Liu, X.F., Song, D.Z., He, X.Q., Nie, B.S., Wang, L.K., 2019. Insight into the macromolecular structural differences between hard coal and deformed soft coal[J]. *Fuel* 245, 188–197.
- Okolo, G.N., Everson, R.C., Neomagus, H.W.J.P., Roberts, M.J., 2015. Comparing the porosity and surface areas of coal as measured by gas adsorption, mercury intrusion and SAXS techniques[J]. *Fuel* 141, 293–304.
- Prins, M.J., Ptasiński, K.J., Janssen, F.J.J.G., 2007. From coal to biomass gasification: comparison of thermodynamic efficiency[J]. *Energy* 32 (7), 1248–1259.
- Schure, M., Soltys, P.A., Natusch, D.F.S., Mauney, T., 1985. Surface area and porosity of coal fly ash[J]. *Environ. Sci. Tech.* 19 (1), 82–86.
- Shen, B., Duan, Y., Luo, X., 2020. Monitoring and modelling stress state near major geological structures in an underground coal mine for coal burst assessment[J]. *Int. J. Rock Mech. Min. Sci.* 129, 104294.
- Shi, Q.L., Qin, B.T., Liang, H.J., Gao, Y., Bi, Q., Qu, B., 2018. Effects of igneous intrusions on the structure and spontaneous combustion propensity of coal: a case study of bituminous coal in Daxing Mine, China[J]. *Fuel* 216, 181–189.
- Shi, Q.L., Jiang, W., Qin, B., Hao, M., 2023. Effects of oxidation temperature on microstructure and spontaneous combustion characteristics of coal: a case study of shendong long-flame coal[J]. *Energy* 284, 128631.
- Wang, Z.Y., Cheng, Y.P., Wang, L., Zhou, H.X., He, X.X., Yi, M.H., Xi, C.P., 2020. Characterization of pore structure and the gas diffusion properties of tectonic and intact coal: Implications for lost gas calculation[J]. *Process Saf. Environ. Prot.* 135 (C), 12–21.
- Wang, K., Dong, H., Wang, L., 2023. Temperature-induced micropore structure alteration of raw coal and its implications for optimizing the degassing temperature in pore characterization[J]. *Energy* 268, 126668.
- Wang, H.Y., Tan, B., Shao, Z.Z., Guo, Y., Zhang, Z.L., Xu, C.F., 2021. Influence of different content of FeS₂ on spontaneous combustion characteristics of coal[J]. *Fuel* 288, 119582.
- Yang, T.T., Xu, G.Q., Chen, K., Sun, G., Dang, B., Liu, M., 2023. Characteristics and evolution of karst collapse columns in the Huainan coalfield.[J]. *Sci. Total Environ.*
- Yin, S.X., Wu, Q., Wang, S.X., 2005. Water-bearing characteristics and hydro-geological models of karstic collapse columns in north China [J]. *Chin. J. Rock Mech. Eng.* 01, 77–82.
- Yu, M.G., Zheng, Y.N., Lu Chang, L.C., Jia, H.L., 2009. Experiment research on coal spontaneous combustion characteristics by TG-FTIR [J]. *J. Henan Polytech. Univ. (Nat. Sci.)* 28 (05), 547–551.
- Yuan, S., Liu, J.Z., Zhu, J.F., 2016. Effect of microwave irradiation on the propensity for spontaneous combustion of Inner Mongolia lignite[J]. *J. Loss Prev. Process Ind.* 44, 390–396.
- Zhang, J., 2022. Generation and Adsorption Mechanism of Coal Spontaneous Combustion Index Gases and Goaf Dangerous Zones Classification Division [D]. Liaoning Technical University.
- Zhang, K.Z., Wang, L., Cheng, Y.P., Li, W., Kan, J., Tu, Q.Y., Jiang, J.Y., 2020. Geological control of fold structure on gas occurrence and its implication for coalbed gas outburst: case study in the Qinan coal mine, Huabei coalfield, China[J]. *Nat. Resour. Res.* 29, 1375–1395.
- Zhao, W.B., Zhang, S.Y., Wang, J.F., Xin, G., 2012. Research on spontaneous combustion tendency of No.3 coal about complex seam under different geological structure in Xin'an Coal Mine [J]. *J. China Coal Soc.* 37 (S2), 346–350. <https://doi.org/10.13225/j.cnki.jccs.2012.s2.040>.